2011 American Control Conference
on O'Farrell Street, San Francisco, CA, USA
June 29 - July 01, 2011

Vision Based Trajectory Tracking of Space Debris in Close Proximity via Integrated Estimation and Control

Ni Li, Yunjun Xu, Gareth Basset, and Norman Fitz-Coy

***Abstract*—The increasingly cluttered environment in space is placing a premium on techniques capable of tracking and estimating the trajectory of space debris. Unlike the debris smaller than 1 cm or larger than 10 cm, it is always a challenge for spacecraft or satellite mission designers to consider explicitly the ones ranged from 1 cm to 10 cm *a priori*. To tackle this challenge, this paper presents a vision based debris' trajectory tracking method in close proximity using two cameras onboard satellites in a formation. Also to differentiate the target debris from other clutters, data association is investigated. A two-stage nonlinear robust controller is developed to adjust the attitude of the satellites such that the desired field of view can be achieved for the target debris. Capabilities of the proposed integrated estimation and control methods are validated in the simulations.**

***Index Terms*—space debris, vision based estimation, robust control, data association.**

I. Introduction

Currently, there are more than million pieces of debris orbiting the Earth every day, and they have already and will continue to threaten human activities in space exploration. Among debris, the pieces smaller than 1cm are unable to damage spacecraft because of the crafts' shields, while the pieces larger than 10cm can be tracked by ground-based radars or a radar network, such as the US SPACECOM [1-3]. Outside of these two groups, it remains a challenge for spacecraft or satellite mission designers to explicitly consider *a priori* the debris ranging from 1 cm to 10 cm. In order to track debris with a size within the range of 1 to 10 cm and in turn reduce the risk of collision, it is preferable that future spacecraft and satellites have the capability of estimating and tracking debris in close proximity autonomously without consistent communication with group stations.

In this paper, an integrated vision based estimation and control approach is proposed to estimate the orbital information of the target debris via cameras aboard the cooperative satellites in a formation. Three technical challenges are specifically addressed and solved in this paper. First, successive 2D images obtained through the vision sensors (e.g. light weight and low cost pinhole cameras) on two satellite platforms are coordinated to obtain the 3D position information of the debris. Second, to maintain the target debris within the cameras' fields of view, the attitude of the satellites is controlled via a two-stage global asymptotically stable nonlinear robust tracking controller [4-10]. Third, because it is possible for multiple debris pieces to appear in the picture frames, a probability data association (PDA) technique [11] combined with the Kalman filter [12] is investigated to differentiate the target debris from the clutter.

The remainder of the paper is organized as follows. Section II describes the overall structure of the integrated sensing and control strategy. The cooperative estimation is described in Section III, which includes the problem definition, Kalman filter, and PDA designs. In Section IV, a nonlinear robust controller is described to maintain the debris inside of the cameras' fields of view. The simulation results are shown in Section V. Conclusion will be drawn in Section VI.

II. Overall Structure

The overall structure of the integrated approach in estimating debris' trajectory is illustrated in Fig. 1. To obtain the 3D position information of the debris, two cooperative satellites, each equipped with a pinhole camera, are used. The debris' projected pixel locations on the focal plane are used as the measurements of cameras. The PDA technique is designed in a decentralized approach to associate each of the possible measurements to the target of interest with a probability. After that, a Kalman filter based on the small disturbance model is designed to estimate the orbit of the debris in a centralized approach. In the meantime, the attitudes of small satellites are controlled coherently such that the target debris is always inside of these two cameras' fields of view.

This work was supported by the Florida Space Grant Consortium Research Grant # 16299904-Y5.

N. Li is with the Department of Mechanical, Materials, and Aerospace Engineering, University of Central Florida, Orlando, FL 32816 USA. (email: xiaonizi_421@knights.ucf.edu)

Y. Xu is with the Department of Mechanical, Materials, and Aerospace Engineering, University of Central Florida, Orlando, FL 32816 USA. Phone: 407-823-1745; Fax: 407-823-0208; (email: yunjunxu@mail.ucf.edu).

G. Basset is with the Department of Mechanical, Materials, and Aerospace Engineering, University of Central Florida, Orlando, FL 32816 USA. (email: gbasset@knights.ucf.edu)

N. Fitz-Coy is with the Department of Aerospace and Mechanical Engineering, University of Florida, Gainesville, FL, 32611, USA. (nfc@ufl.edu)

III. Cooperative Estimation of Debris' Orbit in Clutters

A. Problem Definition of the Cooperative Estimation

The motion of the debris with an altitude larger than 200 km is governed by the following equation

$$\dot{\boldsymbol{r}}_d = \boldsymbol{v}_d; \quad \dot{\boldsymbol{v}}_d = -\left(\mu / r_d^3\right)\boldsymbol{r}_d + \boldsymbol{w} \tag{1}$$

in which the subscript d denotes the debris, $\boldsymbol{r}_d \in \Re^{3\times 1}$ and $\boldsymbol{v}_d \in \Re^{3\times 1}$ represent the position and velocity vectors of the debris in the Earth Centric Inertial (ECI) coordinate, respectively. r_d is the magnitude of the position vector. μ is the gravitational parameter of the Earth. The drag, solar radiation pressure, and higher order gravitational terms, such as the J_2 perturbation are regarded as noise and represented by $\boldsymbol{w}$. Here $\boldsymbol{w}(t)$ is the vector of the zero-mean Gaussian process with an autocorrelation of $E[\boldsymbol{w}(t)\boldsymbol{w}(\tau)^T] = \mathbf{Q}(t)\delta(t-\tau)$.

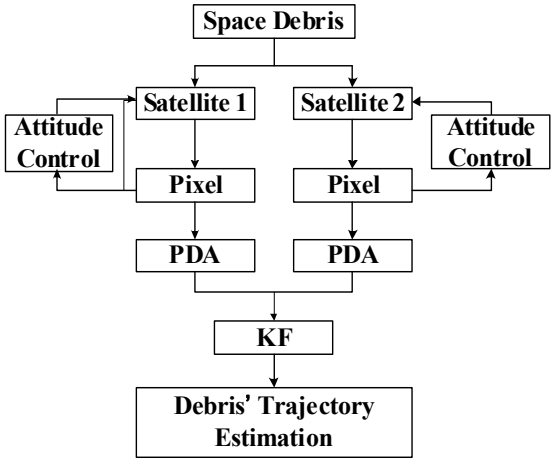

Fig. 1 Overall Structure

Here the small disturbance model derived based upon Eq. (1) is used as the processing dynamics in the PDA-KF design. Let's denote Eq. (1) as $\dot{\boldsymbol{x}}_d = \boldsymbol{f}(\boldsymbol{x}_d) + \boldsymbol{w}$, in which $\boldsymbol{x}_d = [\boldsymbol{r}_d, \boldsymbol{v}_d]^T$. The nominal model is $\dot{\boldsymbol{x}}_{d,0} = \boldsymbol{f}(\boldsymbol{x}_{d,0})$, in which the subscript "0" is used to denote the nominal values. The small disturbance model can be derived as $\Delta\dot{\boldsymbol{x}}_d = \boldsymbol{A}\Delta\boldsymbol{x}_d + \boldsymbol{w}$, where $\boldsymbol{A} = (\partial \boldsymbol{f} / \partial \boldsymbol{x}_d)\big|_{\boldsymbol{x}_{d,0}}$ and $\Delta\boldsymbol{x}_d = \boldsymbol{x}_d - \boldsymbol{x}_{d,0}$.

The measurement is the pixel location of the debris' position projected on the focal plane of the camera onboard of the small satellite. The projection involves a series of coordinate transformations from the ECI, through the local vertical local horizontal (LVLH) coordinate of the satellite, the body coordinate of the satellite, the body coordinate of the camera, and the focal plane of the camera, to the pixel plane of the camera. The detailed coordinate transformations are omitted here, described next.

The position of the debris expressed in the LVLH can be written as

$${}^{(LVLH)}\boldsymbol{r}_{d/s} = \boldsymbol{C}_3(\nu+\omega)\boldsymbol{C}_1(i)\boldsymbol{C}_3(\Omega)\,{}^{(ECI)}\boldsymbol{r}_{d/s} \tag{2}$$

in which $\boldsymbol{r}_{d/s} \triangleq \boldsymbol{r}_d - \boldsymbol{r}_s$, and the subscript "$s$" represents the satellite. ${}^{(ECI)}\boldsymbol{r}_{d/s}$ is the relative position between the debris and the satellite expressed in ECI. In this paper, we use $\boldsymbol{C}_\vartheta(\kappa)$ to denote the direct cosine matrix rotating about the axis ϑ (i.e. 1, 2, or 3) with an angle of κ. In Eq. (2), ν, ω, i, and Ω are the true anomaly, argument of periapsis, inclination, and right ascension of the satellite orbit. The orbit elements of the small satellites are assumed to be constant in this paper.

The relative position of the debris to the satellite $\boldsymbol{r}_{d/s}$ expressed in the body coordinate of the satellite can be written as

$${}^{(B)}\boldsymbol{r}_{d/s} = \boldsymbol{C}_1(\phi)\boldsymbol{C}_2(\theta)\boldsymbol{C}_3(\psi)\,{}^{(LVLH)}\boldsymbol{r}_{d/s} \tag{3}$$

where the superscript "B" denotes the satellite body coordinate. The attitude of the small satellite is represented by the Euler angles $\boldsymbol{\sigma}_s = [\phi, \theta, \psi]^T$, with a rotation sequence of 3-2-1.

The attitude motion of the small satellite is governed by

$$\dot{\boldsymbol{\sigma}}_s = \boldsymbol{R}_1^{-1}\boldsymbol{\omega}_s; \quad \dot{\boldsymbol{\omega}}_s = -\boldsymbol{J}_s^{-1}\tilde{\boldsymbol{\omega}}_s\boldsymbol{J}_s\boldsymbol{\omega}_s + \boldsymbol{J}_s^{-1}\boldsymbol{T} \tag{4}$$

where $\boldsymbol{\omega}_s = [\omega_1, \omega_2, \omega_3]^T$ represents the angular velocity of the satellite. $\boldsymbol{J}_s$ is the moment of inertia of the satellite, and $\boldsymbol{T}$ is the control torque applied. It is worth noting that in both the estimation and control periods of the debris tracking mission, the rotation angle will be kept far away from 90°, therefore the singularity associated with the Euler representation case can be avoided. $\boldsymbol{R}_1$ is the rotation matrix with sequence of 3-2-1, and $\boldsymbol{\omega}_s$ is the skew matrix of the angular velocity.

The relative position $\boldsymbol{r}_{d/s}$ expressed in the camera coordinate, denoted by the superscript "c", is

$${}^{(C)}\boldsymbol{r}_{d/s} = [{}^{(C)}x_{d/s}, {}^{(C)}y_{d/s}, {}^{(C)}z_{d/s}]^T = \boldsymbol{R}_2\,{}^{(B)}\boldsymbol{r}_{d/s} + \boldsymbol{b}_{c/s} \tag{5}$$

As demonstrated in Fig. 2, $\boldsymbol{b}_{c/s}$ is the translational bias between the camera and satellite body coordinate, and $\boldsymbol{R}_2$ is the direct cosine matrix rotating from the satellite body coordinate to the camera coordinate. Without loss of generality, the camera is assumed to be installed along the negative y-axis of the satellite body coordinate, thus the rotation matrix $\boldsymbol{R}_2$ is

$$\boldsymbol{R}_2 = \begin{bmatrix} 1 & 0 & 0 \\ 0 & 0 & 1 \\ 0 & -1 & 0 \end{bmatrix} \tag{6}$$

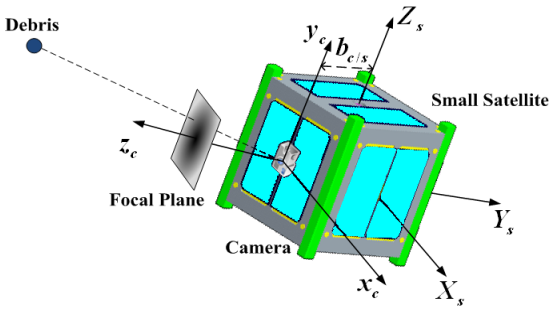

Fig.2 Camera Model

Finally, the pixel location of the debris, $[p_x, p_y]^T$, projected on the focal plane of the camera onboard, is calculated by,

$$p_x = k_1 f_c \frac{^{(C)}x_{d/c}}{^{(C)}z_{d/c}};\ \ p_y = k_2 f_c \frac{^{(C)}y_{d/c}}{^{(C)}z_{d/c}} \tag{7}$$

where f_c is the focal length of the camera, k_1 is the ratio of the length of focal plane and length of pixel plane, and k_2 is the ratio of the width of focal plane and width of pixel plane.

Through Eqs. (2)-(7), the measurement $[p_x, p_y]^T$ can be formulated as a function of $\boldsymbol{x}_d$, $\boldsymbol{x}_s$, and $\boldsymbol{\sigma}_s$ as $\boldsymbol{y} = \boldsymbol{h}(\boldsymbol{x}_d, \boldsymbol{x}_s, \boldsymbol{\sigma}_s) + \boldsymbol{v}(t)$, in which the noise $\boldsymbol{v}(t)$ associated with the measurement is assumed to be a zero-mean Gaussian process with an autocorrelation of $E[\boldsymbol{v}(t)\boldsymbol{v}(\tau)^T] = \boldsymbol{R}(t)\delta(t-\tau)$. Correspondingly, the nominal measurement model is $\boldsymbol{y}_0 = \boldsymbol{h}(\boldsymbol{x}_{d,0}, \boldsymbol{x}_s, \boldsymbol{\sigma}_s)$, and the small disturbance model is derived as $\Delta\boldsymbol{y} = \boldsymbol{H}\Delta\boldsymbol{x}_d + \boldsymbol{v}$, where $\boldsymbol{H} = (\partial\boldsymbol{h}/\partial\boldsymbol{x}_d)\big|_{\boldsymbol{x}_{d,0}}$ and $\Delta\boldsymbol{y} = \boldsymbol{y} - \boldsymbol{y}_0$ [12].

B. Probability Data Association Filter

For brevity, only an outline of how to apply the PDA technique in this specific problem is given. The detailed information about the PDA method can be found in [11].

In each sampling time k, a validation set, defined by Eq. (8), is created, and only the measurements satisfying the constraint in Eq. (8) are considered as the validated measurements, while the other measurements will be discarded.

$$Z_k \triangleq \{\boldsymbol{y}_{i,k} : \boldsymbol{d}_{i,k}^T(k)\boldsymbol{S}_k^{-1}\boldsymbol{d}_{i,k} \le \gamma\},\ i = 1,...,m_k \tag{8}$$

Here, γ and m_k are the threshold of the validation set and the number of the measurements in the validation set at time step k, respectively. γ can be chosen according to the Chi Square distribution as described in [11], and the innovation $\boldsymbol{d}_{i,k}$ is

$$\boldsymbol{d}_{i,k} = \boldsymbol{y}_{i,k} - \hat{\boldsymbol{y}}_{k|k-1},\ i = 1,...,m_k \tag{9}$$

in which $\hat{\boldsymbol{y}}_{k|k-1}$ is the predicted measurement at step k based on the estimated value obtained at step $k-1$. The cumulative set of measurements in the validated region up to the sampling time k is defined to be $Z^k \triangleq \{Z_j, j = 1,...k\}$.

Now, let's define the following two events: (1) Event $\theta_{i,k}$ is defined as the case when the validated measurement $\boldsymbol{y}_{i,k} \in Z_k$ is originated from the target debris. The conditional probability of this event $\beta_{i,k}$ is calculated by

$$\beta_{i,k} \triangleq P(\theta_{i,k} \mid Z^k) = e_{i,k} / (b + \sum_{j=1}^{m_k} e_{j,k}),\quad i = 1,...,m_k \tag{10}$$

(2) Event $\theta_{0,k}$ is defined as the case when none of the validated measurement $\boldsymbol{y}_{i,k} \in Z_k$ is originated from the target debris, and the corresponding conditional probability $\beta_{0,k}$ is

$$\beta_{0,k} \triangleq P(\theta_{0,k} \mid Z^k) = b / (b + \sum_{j=1}^{m_k} e_{j,k}) \tag{11}$$

In Eqs. (10) and (11),

$$e_{j,k} = \exp\{-\frac{1}{2}\boldsymbol{d}_{j,k}^{'}\boldsymbol{S}_k^{-1}\boldsymbol{d}_{j,k}\} \tag{12}$$

$$b = (2\pi/\gamma)^{n_z/2} m_k C_{n_z}(1 - P_D P_G)/P_D \tag{13}$$

Here, n_z is the dimension of the measurement (i.e. two for the problem in this paper) and C_{n_z} is the volume of the n_z dimensional unit hyper sphere (i.e. $C_{n_z} = \pi$ if $n_z = 2$). P_G is the probability that the measurement will fall in the threshold gate, and it will be fixed once γ and n_z are given. P_D is the probability that the true measurement is detected [11].

The measurement prediction covariance $\boldsymbol{S}_k$ used in Eq. (8), is propagated through

$$\boldsymbol{S}_k = \boldsymbol{H}_k \boldsymbol{P}_{k|k-1} \boldsymbol{H}_k^T + \boldsymbol{R} \tag{14}$$

and

$$\boldsymbol{P}_{k|k-1} = \boldsymbol{A}_{k-1} \boldsymbol{P}_{k-1|k-1} \boldsymbol{A}_{k-1}^T + \boldsymbol{Q} \tag{15}$$

respectively. The update equation of the error covariance is

$$\boldsymbol{P}_{k|k} = \beta_{0,k}\boldsymbol{P}_{k|k-1} + (1-\beta_{0,k})\boldsymbol{P}_{k|k}^c + \tilde{\boldsymbol{P}}_k \tag{16}$$

where

$$\tilde{\boldsymbol{P}}_k = \boldsymbol{K}_k[\sum_{i=1}^{m_k}\beta_{i,k}\boldsymbol{d}_{i,k}\boldsymbol{d}_{i,k}^T - \boldsymbol{d}_k\boldsymbol{d}_k^T]\boldsymbol{K}_k^T \tag{17}$$

$$\boldsymbol{d}_k = \sum_{i=1}^{m_k}\beta_{i,k}\boldsymbol{d}_{i,k} \tag{18}$$

and the error covariance of the measurement that possibly originated from the target debris is

$$\boldsymbol{P}_{k|k}^c = (1 - \boldsymbol{K}_k\boldsymbol{H}_k)\boldsymbol{P}_{k|k-1} \tag{19}$$

In Eq. (19), $\boldsymbol{K}_k$ is the Kalman gain.

Then the updated states of the small disturbance model is given by

$$\Delta\hat{\boldsymbol{x}}_{d,k|k} = \Delta\hat{\boldsymbol{x}}_{d,k|k-1} + \boldsymbol{K}_k\boldsymbol{d}_k \tag{20}$$

At each step, once the small disturbance $\Delta\hat{\boldsymbol{x}}_{d,k|k}$ is updated,

the estimated position of the debris can be calculated via

$$\hat{\boldsymbol{x}}_{d,k} = \boldsymbol{x}_{d,0,k} + \Delta\hat{\boldsymbol{x}}_{d,k|k} \tag{21}$$

in which $\boldsymbol{x}_{d,0,k}$ is the nominal value of the debris' trajectory at time step k [12].

IV. Nonlinear Robust Attitude Control

If the projected pixel location of the debris is very close to the boundary of the camera's field of view, the direction of camera, thus the attitude of the small/micro satellite, needs to be controlled such that the projected pixel location of the debris on the focal plane can be driven to a desired location, e.g. the center of the image.

In this work, we will employ a newly developed nonlinear robust control technique to solve this problem. Here only the main steps and equations are listed, and the detailed theorem and asymptotically stability proof can be found in [5-6].

A. Stage 1: Projected Pixel Tracking Control

In this stage, the pixel location of the debris is driven to the desired position, e.g. the center of the image plane. At the same time, the angular velocity of the satellite is regulated to zero.

Equation (4) is the state dynamics, in which the transpose of the input matrix $\boldsymbol{B}^T$ is $[\boldsymbol{0}, \boldsymbol{J}_s^{-1}]$. The state functions $\boldsymbol{f}$ includes two parts: $\boldsymbol{f}_1 = \boldsymbol{R}_1^{-1}\boldsymbol{\omega}_s$ and $\boldsymbol{f}_2 = -\boldsymbol{J}_s^{-1}\tilde{\boldsymbol{\omega}}_s\boldsymbol{J}_s\boldsymbol{\omega}_s$. The output of the controlled system is

$$\boldsymbol{y} = \begin{bmatrix} \boldsymbol{y}_1 \\ \boldsymbol{y}_2 \end{bmatrix} = \begin{bmatrix} \boldsymbol{h}_1 \\ \boldsymbol{h}_2 \end{bmatrix} \tag{22}$$

in which $\boldsymbol{h}_1$ is the pixel location of the debris position and $\boldsymbol{h}_2$ is the angular velocity of the satellites.

The relative degree $\boldsymbol{r}$ of this system is $[2 \quad 2 \quad 1 \quad 1 \quad 1]^T$, and according to Theorem 1, the nonlinear robust controller has the following simplified form

$$\boldsymbol{u} = \begin{bmatrix} L_{\hat{\boldsymbol{B}}}L_{\hat{\boldsymbol{f}}}\hat{\boldsymbol{h}}_1 \\ L_{\hat{\boldsymbol{B}}}\hat{\boldsymbol{h}}_2 \end{bmatrix}^{+} \left\{ \begin{bmatrix} \dfrac{d^2\boldsymbol{y}_{1,des}}{dt^2} \\ \dfrac{d\boldsymbol{y}_{2,des}}{dt} \end{bmatrix} - \begin{bmatrix} L_{\hat{\boldsymbol{f}}}^2\hat{\boldsymbol{h}}_1 \\ L_{\hat{\boldsymbol{f}}}\hat{\boldsymbol{h}}_2 \end{bmatrix} + \boldsymbol{\lambda}_{-1} \cdot \begin{bmatrix} \boldsymbol{e}_1 \\ \boldsymbol{e}_2 \end{bmatrix} + \begin{bmatrix} \boldsymbol{\lambda}_0 \cdot \boldsymbol{e}_1 \\ \boldsymbol{0} \end{bmatrix} + \boldsymbol{k} \cdot \boldsymbol{s} \right\} \tag{23}$$

where

$$L_{\hat{\boldsymbol{B}}}L_{\hat{\boldsymbol{f}}}\hat{\boldsymbol{h}}_1 = \frac{\partial}{\partial\hat{\boldsymbol{\omega}}_s}\left(\frac{\partial\hat{\boldsymbol{h}}_1}{\partial\hat{\boldsymbol{\sigma}}_s}\hat{\boldsymbol{f}}_1\right)\boldsymbol{J}_s^{-1} = \frac{\partial\hat{\boldsymbol{h}}_1}{\partial\hat{\boldsymbol{\sigma}}_s}\hat{\boldsymbol{R}}_1^{-1}\boldsymbol{J}_s^{-1} \tag{24}$$

$$L_{\hat{\boldsymbol{B}}}\hat{\boldsymbol{h}}_2 = \boldsymbol{J}_s^{-1} \tag{25}$$

$$L_{\hat{\boldsymbol{f}}}^2\hat{\boldsymbol{h}}_1 = \frac{\partial}{\partial\hat{\boldsymbol{\sigma}}_s}\left(\frac{\partial\hat{\boldsymbol{h}}_1}{\partial\hat{\boldsymbol{\sigma}}_s}\hat{\boldsymbol{R}}_1^{-1}\hat{\boldsymbol{\omega}}_s\right)\hat{\boldsymbol{R}}_1^{-1}\hat{\boldsymbol{\omega}}_s - \frac{\partial\hat{\boldsymbol{h}}_1}{\partial\hat{\boldsymbol{\sigma}}_s}\hat{\boldsymbol{R}}_1^{-1}\boldsymbol{J}_s^{-1}\tilde{\hat{\boldsymbol{\omega}}}_s\boldsymbol{J}_s\hat{\boldsymbol{\omega}}_s \tag{26}$$

$$L_{\hat{\boldsymbol{f}}}\hat{\boldsymbol{h}}_2 = \frac{\partial\hat{\boldsymbol{h}}_2}{\partial\hat{\boldsymbol{\omega}}_s}\hat{\boldsymbol{f}}_2 \tag{27}$$

$$\boldsymbol{s} = \begin{bmatrix} \boldsymbol{s}_1 \\ \boldsymbol{s}_2 \end{bmatrix} = \boldsymbol{\lambda}_{-1} \cdot \begin{bmatrix} \int \boldsymbol{e}_1 dt \\ \int \boldsymbol{e}_2 dt \end{bmatrix} + \begin{bmatrix} \boldsymbol{\lambda}_0 \cdot \boldsymbol{e}_1 \\ \boldsymbol{0} \end{bmatrix} + \begin{bmatrix} \dot{\boldsymbol{e}}_1 \\ \boldsymbol{e}_2 \end{bmatrix} \tag{28}$$

and

$$\begin{bmatrix} \boldsymbol{e}_1 \\ \boldsymbol{e}_2 \end{bmatrix} = \begin{bmatrix} \boldsymbol{y}_{1,des} - \hat{\boldsymbol{y}}_1 \\ \boldsymbol{y}_{2,des} - \hat{\boldsymbol{y}}_2 \end{bmatrix} \tag{29}$$

$\boldsymbol{y}_{1,des}$ and $\boldsymbol{y}_{2,des}$ are the desired pixel location and angular velocity, e.g. $[0 \quad 0]^T$ and $[0 \quad 0 \quad 0]^T$.

The control gain $\boldsymbol{k} = [k_1, ..., k_5]^T$ are obtained from

$$(\boldsymbol{I} - \boldsymbol{D})\boldsymbol{k} \cdot \boldsymbol{s} = \boldsymbol{F} + \boldsymbol{D}\left| \begin{bmatrix} \dfrac{d^2\boldsymbol{y}_{1,des}}{dt^2} \\ \dfrac{d\boldsymbol{y}_{2,des}}{dt} \end{bmatrix} - \begin{bmatrix} L_{\hat{\boldsymbol{f}}}^2\hat{\boldsymbol{h}}_1 \\ L_{\hat{\boldsymbol{f}}}\hat{\boldsymbol{h}}_2 \end{bmatrix} + \boldsymbol{\lambda}_{-1} \cdot \begin{bmatrix} \boldsymbol{e}_1 \\ \boldsymbol{e}_2 \end{bmatrix} + \begin{bmatrix} \boldsymbol{\lambda}_0 \cdot \boldsymbol{e}_1 \\ \boldsymbol{0} \end{bmatrix} \right| + \boldsymbol{\eta} \cdot \boldsymbol{s} \tag{30}$$

and in the stage 1 controller

$$\boldsymbol{F} = \left| -\begin{bmatrix} L_f^2\boldsymbol{h}_1 \\ L_f\boldsymbol{h}_2 \end{bmatrix} + \begin{bmatrix} L_f^2\hat{\boldsymbol{h}}_1 \\ L_f\hat{\boldsymbol{h}}_2 \end{bmatrix} \right| \tag{31}$$

is assumed to be the error bound between the predicted and actual state function. To guarantee the asymptotically stability, $\boldsymbol{\lambda}_{-1}$, $\boldsymbol{\lambda}_0$ and $\boldsymbol{\eta}$ are required to be positive.

B. Stage 2: Small Satellite Attitude Stabilization

In this stage, the Euler angles of satellite need to be maintained at the fixed value to ensure that the debris will stay within the field of view of camera for a relatively long duration. Eq. (4) is the state equation, while $y_3 = \boldsymbol{h}_3 = \boldsymbol{\sigma}_s$ is controlled to the desired the Euler angle of the satellite $y_{3,des} = \boldsymbol{\sigma}_{s,des}$. The relative degree $\boldsymbol{r}$ of the system is $[2 \quad 2 \quad 2]^T$, and the nonlinear robust controller proposed in Theorem 1 can be simplified as

$$\boldsymbol{u} = \left[L_{\hat{\boldsymbol{B}}}L_{\hat{\boldsymbol{f}}}\hat{\boldsymbol{h}}_3\right]^{-1}\left[\frac{d^2\boldsymbol{y}_{3,des}}{dt^2} - L_{\hat{\boldsymbol{f}}}^2\hat{\boldsymbol{h}}_3 + \boldsymbol{\lambda}_{-1} \cdot \boldsymbol{e}_3 + \boldsymbol{\lambda}_0 \cdot \dot{\boldsymbol{e}}_3 + \boldsymbol{k} \cdot \boldsymbol{s}_3\right] \tag{32}$$

in which

$$L_{\hat{\boldsymbol{B}}}L_{\hat{\boldsymbol{f}}}\hat{\boldsymbol{h}}_3 = \hat{\boldsymbol{R}}_1^{-1}\boldsymbol{J}_s^{-1} \tag{33}$$

$$L_{\hat{\boldsymbol{f}}}^2\hat{\boldsymbol{h}}_3 = \begin{bmatrix} \dfrac{\partial\hat{\boldsymbol{R}}_1^{-1}}{\partial\hat{\boldsymbol{\omega}}_s}\hat{\boldsymbol{\omega}}_s & \hat{\boldsymbol{R}}_1^{-1} \end{bmatrix}\begin{bmatrix} \hat{\boldsymbol{f}}_1 \\ \hat{\boldsymbol{f}}_2 \end{bmatrix} = \frac{\partial\hat{\boldsymbol{R}}_1^{-1}}{\partial\boldsymbol{\sigma}_s}\hat{\boldsymbol{\omega}}_s\hat{\boldsymbol{f}}_1 + \hat{\boldsymbol{R}}_1^{-1}\hat{\boldsymbol{f}}_2 \tag{34}$$

$$\boldsymbol{s}_3 = \boldsymbol{\lambda}_{-1} \cdot \int \boldsymbol{e}_3 dt + \boldsymbol{\lambda}_0 \cdot \boldsymbol{e}_3 + \dot{\boldsymbol{e}}_3 \tag{35}$$

and

$$\boldsymbol{e}_3 = \boldsymbol{y}_{3,des} - \hat{\boldsymbol{y}}_3 \tag{36}$$

in which, $\boldsymbol{y}_{3,des}$ is the Euler angles achieved at the end of control stage 1. The control gain $\boldsymbol{k} = [k_1, k_2, k_3]^T$ needs to satisfy

$$\boldsymbol{F} + \boldsymbol{D}\left|\frac{d^2\boldsymbol{y}_{3,des}}{dt^2} - L_{\hat{\boldsymbol{f}}}^2\hat{\boldsymbol{h}}_3 + \boldsymbol{\lambda}_{-1} \cdot \boldsymbol{e}_3 + \boldsymbol{\lambda}_0 \cdot \dot{\boldsymbol{e}}\right| + \boldsymbol{\eta} \cdot \boldsymbol{s}_3 = (\boldsymbol{I} - \boldsymbol{D})\boldsymbol{k} \cdot \boldsymbol{s}_3 ($$

37)

V. Numerical Simulation

A. Simulation Scenario

The orbital information of the two micro satellites and the debris used in the simulation are listed in Table 1. It is assumed that initially both satellites have zero Euler angles and angular velocities. The moment of inertia of the satellite is obtained from the satellite platform developed at the University of Central Florida as

$$\boldsymbol{J}_s = \begin{bmatrix} 10662.54 & -40.20 & 73.65 \\ -40.20 & 10415.43 & 48.15 \\ 73.65 & 48.15 & 9618.74 \end{bmatrix} (\mathrm{g}\cdot\mathrm{cm}^2) \quad (38)$$

To demonstrate the effectiveness of the data associate technique applied in this paper, two interference debris, i.e. two clutters, are generated around the target debris randomly.

Table 1. Orbital information of the satellites and debris

Orbital information	Satellite 1/2, debris
Inclination	$30^\circ / 30^\circ,\ 20^\circ$
Semi-major axis (km)	7500/7500, 7493
Eccentricity	0.1/0.1, 0.1
Right ascension	$10^\circ / 7^\circ,\ 35^\circ$
Initial true anomaly	$8^\circ / 8^\circ,\ 8^\circ$
Argument of periapsis	$90^\circ / 90^\circ,\ 70^\circ$

The camera is located along the negative y axis of the satellite as shown in Fig. 2 with a focal length of $0.1m$, and the resolution of the images is chosen to be 480×360. The tuned parameters for the data association, estimation, and controller are listed in Table 2. In the estimation part, the Gaussian noise associated with the processing dynamics is assumed to have a zero mean and covariance matrix of $\boldsymbol{Q} = 10^{-8}\boldsymbol{I}_3\ \mathrm{km}^2/s^4$ and Gaussian noise associated with measurement is assumed to have a zero mean and covariance matrix of $\boldsymbol{R} = \boldsymbol{I}_2$. The initial error covariance matrix is set as $0.01\boldsymbol{I}_6$.

Table 2. Parameters used in the estimation and control

Estimation	Value	Estimation	Value
P_G	0.9	γ	5
P_D	0.7	n_Z	4
Control		Stage 1/2	
$\boldsymbol{\lambda}_{-1}$	$[5,5,1,1,1]^T$ / $[10\ \ 10\ \ 10]^T$		
$\boldsymbol{\lambda}_0$	$[3,3]^T$ / $[1\ \ 1\ \ 1]^T$		
$\boldsymbol{\eta}$	$[0.1,0.1,0.001,0.0005,0.001]^T$ / $[0.001\ \ 0.001\ \ 0.001]^T$		

The following uncertainties have been considered in the control section: the Euler angle is assumed to have 5% percentage errors, while errors in the angular velocity measurement are assumed to be 5%. Also the pixel location of the debris is the rounded to the nearest integer. The analytical bounds of $\boldsymbol{F}$ and $\boldsymbol{D}$ cannot be derived easily, so the Monte Carlo simulation is conducted in this paper and $\boldsymbol{F}$ and $\boldsymbol{D}$ are found to be $0.1\left|L_{\hat{f}}^2\hat{\boldsymbol{h}}_3\right|$ and $0.4\boldsymbol{I}_3$ approximately.

B. Simulation Results

As shown in Figs. 3-5, the debris is initially inside of the two cameras' fields of view, thus the data associate and estimation methods are activated to estimate the debris' trajectory among the clutters. Then, when the pixel location of the debris of Satellite two is close to the boundary of the focal planes, the attitude control of both satellites are activated simultaneously such that the pixel locations of the debris are driven to the center of image, i.e. $[0,0]$, and the angular velocities of the satellites are controlled simultaneously to zero. After that, the estimation is resumed to track the target debris until the debris is out of camera's fields of view and attitude controllers are activated again. The estimation section is marked as "E", while the control section is marked as "C".

As shown in Fig. 5, initially the target debris is close to the image boundary of the camera on the second satellite, therefore the estimation in the first "E" section is not fully settled down as shown in Figs. 3 and 4 within only 25 seconds. The capability of the proposed integrated approach is illustrated through the following section "C" and section "E". The pixel locations of the target debris on two cameras are driven to the center, and the estimation error and the trace value of the error covariance matrix can reach their steady state in a relatively long duration before the debris drifts to the boundary of the image again.

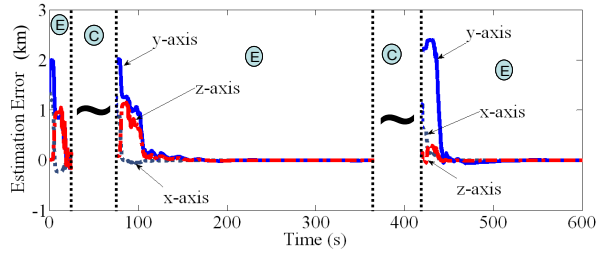

Fig. 3 Estimation error of the target debris' trajectory

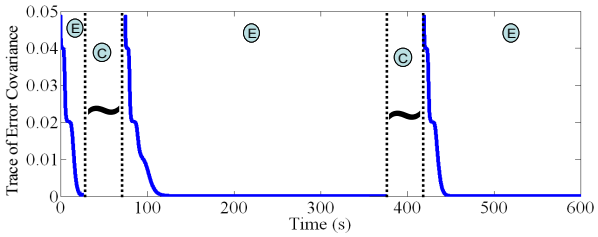

Fig. 4 Trace of the error covariance matrix

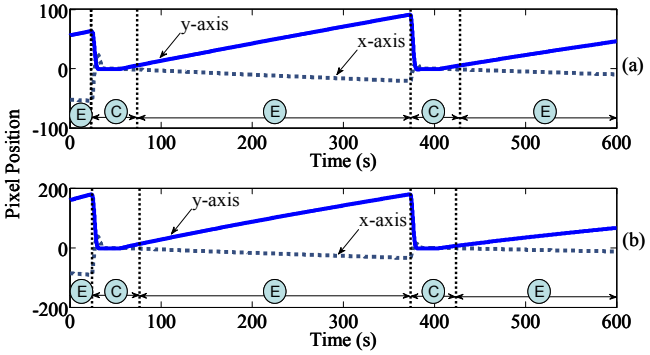

Fig. 5 The pixel locations of the debris on the focal plane of: a) Satellite one; b) Satellite two.

It is worth noting that the pixel locations in Fig. 5 begin to drift in the final part of control section. The reason is that the debris is always moving, thus the projected pixels will be moving from desired location over time if only the attitude of the satellites is maintained in stage two.

The performance of torque commands in the control is listed in the Fig. 6 and Fig. 7, the torque commands do not have high frequency chatters.

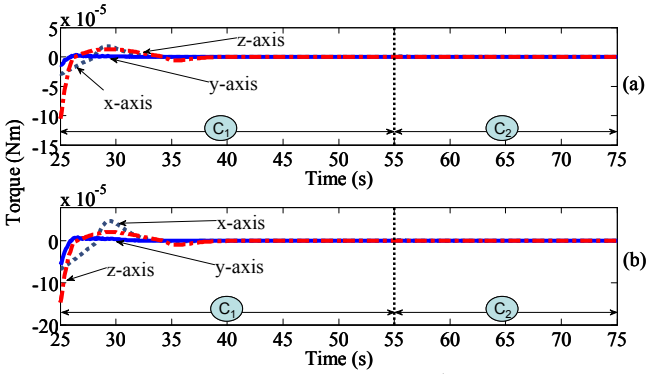

Fig. 6 Torque commands during the 1st attitude control period: a) Satellite one; b) Satellite two

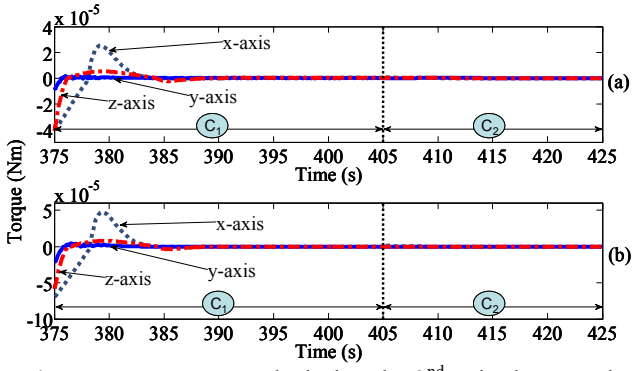

Fig. 7 Torque commands during the 2nd attitude control period: a) Satellite one; b) Satellite two

VI. Conclusion

In this paper, a vision based method, using 2D cameras aboard two satellites in a formation, is presented to track the debris in close proximity. As compared with the other approaches such as using SAR, ISAR or a stereo camera on a single large satellite, the proposed method has the following advantages: cost reduction, avoidance of reconstruction of images, increased mission flexibility and observational baseline, and better survivability and reliability. Three technical issues are specifically addressed for: successive 2D images obtained on two satellite platforms are coordinated to obtain the 3D position information of the debris. The attitude of the satellites is controlled via a two-stage asymptotically stable nonlinear robust tracking controller so that the target debris can be maintained within the cameras' fields of view. The PDA combined with the Kalman filter is developed to differentiate the target debris from the clutter. The simulation results demonstrate the effectiveness of the methodology.

Acknowledgment

The authors would like to thank the anonymous reviewers for their comments and suggestions. Also the authors appreciate the support from Jaydeep Mukherjee through the Florida Space Grant Consortium Research Grant # 16299904-Y5.

References

[1] Loughman, J. J., "Overview and Analysis of the SOLDIER Satellite Concept for Removal of Space Debris," *AIAA SPACE 2010 Conference and Exposition*, Anaheim, California, August 30-September 2, 2010, Paper# AIAA 2010-8909.

[2] Molayath, A., and Khan, Y., "Studies on Space Debris Tracking and Elimination," *46th AIAA/ASME/SAE/ASEE Joint Propulsion Conference and Exhibit*, Nashville, TN, July 25-28, 2010, Paper# AIAA 2010-7008.

[3] Heimerdinger, D.J., "Orbital Debris and Associated Space Flight Risks," *Proceedings of 2005 Annual Reliability and Maintainability Symposium,* Alexandria, Virginia, USA, January 24-27, 2005, pp. 508-513.

[4] Xu, Y., "Sliding Mode Control and Optimization for 6 DOF Satellites' Formation Flying Considering Saturation," *the Journal of Astronautical Science*, Vol. 53, No. 4, October-December, 2005, pp. 433-443.

[5] Xu, Y., "Chattering Free Robust Control for Nonlinear Systems," *IEEE Transactions on Control Systems Technology*, Vol. 16, No. 6, 2008, 2008, pp. 1352-1359.

[6] Xu, Y., "Multi-Timescale Nonlinear Robust Control for a Miniature Helicopter," *IEEE Transaction on Aerospace and Electronic Systems*, Vol. 46, No. 2, 2010, pp. 656-671.

[7] Bartolini, G., Ferrara, A., Usai, E., and Utkin, V. I., "On Multi-input Chattering-free Second Order Sliding Mode Control," *IEEE Transactions on Automatic Control*, Vol. 45, No. 9, Sep. 2000, pp. 1711-1717.

[8] Yao, B., and Tomizuka, M., "Smooth Robust Adaptive Sliding Mode Control of Manipulators with Guaranteed Transient Performance," *2004 American Control Conference*, Baltimore, MD, 1994, pp. 1176-1180.

[9] Krupp, D. R., Shkolnikov, I. a., and Shtessel, Y. B., "High Order Sliding Modes in Dynamic Sliding Manifolds, SMC Design with Uncertain Actuator," *2000 American Control Conference*, Chicago, IL, June 2000, pp. 1124-1128.

[10] Levant, A., "High-order Sliding Modes, Differentiation and Output-feedback Control," *International Journal of Control*, Vol. 76, Issue 9/10, 2003, pp. 924-941.

[11] Bar-Shalom, Y., and Fortmann, T. E., *Tracking and Data Association*, Academic Press, Orlando, FL, 1988.

[12] Simon, D., *Optimal State Estimation*, John Wiley & Sons, Hoboken, NJ, 2006.